Int. J. Radiation Oncology Biol. Phys., Vol. 63, No. 4, pp. 1101–1107, 2005

0360-3016/05/$–see front matter

doi:10.1016/j.ijrobp.2005.03.042

CLINICAL INVESTIGATION **Cervix**

A THREE-DIMENSIONAL DEFINITION OF NODAL SPACES ON THE BASIS OF CT IMAGES SHOWING ENLARGED NODES FOR PELVIC RADIOTHERAPY

MAURIZIO PORTALURI, M.D.,* SANTA BAMBACE, M.D.,* CELESTE PEREZ, M.D.,† AND GRAZIA ANGONE, M.D.†

*Departments of Radiotherapy and †Radiology "Di Summa-A. Perrino" General Hospital, Brindisi, Italy

Purpose: To demonstrate that margins of each pelvic chain may be derived by verifying the bony and soft tissue structures around abnormal nodes on computed tomography (CT) slices.

Methods and Materials: Twenty consecutive patients (16 males, 4 females; mean age, 66 years; range, 43–80 years) with radiologic diagnosis of nodal involvement by histologically proved cervix carcinoma (two), rectum carcinoma (three), prostate carcinoma (four), lymphoma (five), penis carcinoma (one), corpus uteri carcinoma (one), bladder carcinoma (two), cutis tumor (one), and soft-tissue sarcoma (one) were retrospectively reviewed. One hundred CT scans showing 85 enlarged pelvic nodes were reviewed by two radiation oncologists (M.P., S.B.), and two radiologists (C.P., G.A.).

Results: The more proximal structures to each enlarged node or group of nodes were thus recorded in a clockwise direction.

Conclusion: According to their frequency and visibility, craniocaudal, anterior, lateral, posterior and medial margins of common iliac, external and internal iliac nodal chains, obturator and pudendal nodes, and deep and superficial inguinal nodes were derived from CT observations. © **2005 Elsevier Inc.**

Clinical target volume, Radiotherapy, Pelvic nodes, Computed tomography, Three-dimensional conformal radiotherapy.

Improvements in customizing planning target volume by means of intensity modulated radiation therapy, and three-dimensional conformal radiotherapy by the avoidance of organs at risk in all the anatomic districts will lead to a more accurate contouring of nodal clinical target volume (CTV).

Some authors recently proposed a very good definition of CTV in head–and–neck region, which was reached and validated by collecting valuable information from surgical literature and from radiologic series (1–3). Consensus were also achieved among regional radiation oncologists groups (4). In the pelvic region, guidelines for a correct drawing of CTV have also been proposed. They consisted of adding different margins to contrast enhanced vessels (5) and also considering their focal expansion or truncation in computed tomography (CT) and lymphangiography at the same time (6).

Lymph nodes run mostly along the main pelvic arteries, sometimes close to the undetectable ones (e.g., pudendal artery) or independently from arteries (superficial inguinal nodes) and are not visible on CT slices if they are not enlarged. For this reason, we started to prove the hypothesis suggested to define the marginal structures of each nodal chain in CT cross sections as borders of nodal CTV and places where subclinical malignant disease might be situated (7). Therefore, to determine the relative positions of nodes on cross-sectional CT, pelvic CT exams with IVM performed, during 8 months, in patients with pathologically proven cancer and referred to this radiotherapy (RT) department for consultation (pre-RT) or follow-up (post-RT) were collected. Only CT scans with evidence of enlarged pelvic nodes were considered for this study. On CT, images of anatomic structures located in proximity to enlarged pelvic lymph nodes were identified and listed.

The aim of the study was to demonstrate that boundaries of enlarged pelvic nodes on CT scans can help define the three-dimensional margins of pelvic nodal chains. This could be valuable in those locations, such as pudendal and internal chains, where lymphatic contrast does not permit us to see normal nodes. Furthermore, this assertion could be particularly valid when nodes, such as the superficial inguinal ones, are not related to arterial vessels.

METHODS AND MATERIALS

Twenty consecutive patients (16 males, 4 females; mean age, 66 years; range, 43–80 years) with radiologic diagnosis of nodal involve-

Reprint requests to: Maurizio Portaluri, M.D., Department of Radiotherapy, AUSL BR1, Hospital "A. Di Summa-A. Perrino," Strada Statale 7, 72100 Brindisi, Italy. Tel: (+39) 0831-537642; Fax: (+39) 0831-537640; E-mail: portaluri@hotmail.com.

Received Jan 7, 2005, and in revised form Mar 15, 2005. Accepted for publication Mar 16, 2005.

Table 1. Distribution of computed tomography slices and enlarged nodes according to node chains

Node chains	No. slices	No. enlarged nodes
Common iliac	6	5
Superficial inguinal	26	39
Deep inguinal	14	10
External iliac	20	11
Internal iliac	10	5
Pudendal	7	6
Obturator	9	6
Presacral	8	3
Total	100	85

ment by histologically proved carcinoma of the cervix ($n = 2$), carcinoma of the rectum ($n = 3$), carcinoma of the prostate ($n = 4$), lymphoma ($n = 5$), carcinoma of the penis ($n = 1$), carcinoma of the corpus uteri ($n = 1$), carcinoma of the bladder ($n = 2$), cutis carcinoma ($n = 1$), and soft-tissue sarcoma ($n = 1$) were retrospectively reviewed.

In 8 months, CT images were collected among patients referred to this RT department for RT consult or post-RT follow-up. These patients needed CT exams with IVM for RT prescription and stage definition or for outcome evaluation. In this study, those CT scans with enlarged nodes in the regions of nodal pelvic and inguinal chains were considered relevant and selected by two radiologists (G.A., C.P.). Those nodes larger than 1 cm were defined as "enlarged." They could be metastatic or reactive. However, their pathologic definitions were not considered relevant for our study.

Helical CT scans were taken 70 s after IVM injection from the lower pole of kidneys to the superior third of the thigh. All patients were scanned with helical CT (Toshiba model Xpress GX, Toshiba Corp., Tokyo, Japan) using the following parameters: 5-mm collimation, 3-mm reconstruction index, a table speed of 7 mm/s, 120 kVp, and 200–250 mA. Intravenous injection (2 mL/kg of body weight) of Ultravist 370 (Schering AG, Berlin, Germany) by

Table 2. Marginal structures and their occurrence for each pelvic nodal chain

Anterior		Lateral		Posterior		Medial	
Common iliac nodes ($n = 5$)							
Ureter	1	Psoas m.	4	Psoas m.	1	Caval vein	5
Mesocolon	4	Mesocolon	1	Sacral bone	4		
External iliac nodes ($n = 11$)							
Spermatic cord	2	Ileopsoas m.	5	Pubic bone	3	Bladder	8
Bowel	4	Iliac bone	1	Pelvic fat	2	Ureter	2
Subcutaneous fat	2	External iliac vein	4	Acetabulum	2	Bowel	1
Bladder	2	Psoas	1	Psoas	2		
Recta muscles	1			Iliac vessels	2		
Internal iliac node ($n = 5$)							
Bladder	3	Internal iliac vessels	1	Piriformis m.	5	Uterus	1
Uterus	1	Iliac bone	1			Bladder	1
Urether	1	Obturatorius m.	1			Mesorectum	3
		Piriform m.	2				
Pudendal nodes ($n = 6$)							
Internal obturator m.	5	Gluteus m.	3	Gluteus m.	4	Mesorectum	4
Acetabulum	3	Sciaticus n.	3	Ischiorectal fossa	2	Elevator ani	1
Elevator ani m.	1	Internal obturatorius m.	1			Internal obturator m.	1
Superficial inguinal nodes ($n = 39$)							
Subcutaneous fact	14	M. sartorius	24	Femoral vessels	18	Spermatic cord	18
Cutis	10	Subcutaneus fat	4	M. pectincus	4	Subcutis	3
		Cutis	1	M. ileopsoas	4	M. trasversus ab.	1*
		Rectus femoris m.	1	M. sartorius	4	M. rectus ab.	1*
		Ileopsoas m.	1	M. adductorius	2	Sovrapubic fat	1*
						M. obliquus ab.	1*
Presacral nodes ($n = 3$)							
Posterior rectum wall	1	Piriformis m.	1	Sacral bone (anterior surface)	2		
Small bowel	1	Iliac vessels	1	Wing	1		
Urether	1	Iliac wing	1				
Deep inguinal nodes ($n = 10$)							
Inguinal ring	5	Femural vein	7	M. pectineus	9	Bladder	3
Subcutaneous fat	4	M. sartorius	2	Acetabulum	1	M. pectineus	4
Line along anterior		M. ileopsoas	2			Spermatic cord	4
Surface m. sartorius	2	M. rectus femuri	1			Subcutaneus fat	2
Obturators nodes ($n = 6$)							
Bladder	2	Obturatoris m.	5	Internal obturatorius m.	4	Bladder	4
External iliac vein	2	Acetabulum	1	Post edge acetabulum	1	Uterus	1
Ileopubic bone	1			Seminal vescicle	1	Small bowel	1
Ant edge acetabulum	1						

n = number of observations.
* More cranial slices.

Table 3. Guidelines proposal for pelvic nodes CTV drawing

Node chains	Cranial margin	Caudal margin	Anterior margin	Lateral margin	Posterior margin	Medial margin
Common iliac nodes	Aortic bifurcation	Common iliac bifurcation	Mesocolon	Psoas m	sacrum	
External iliac nodes	Common iliac bifurcations (about L5-S1)	Femoral ring: disappearance of lateral muscles of abdominal wall and artery gets lateral	Fat of small bowel Deferent duct or round legament	Cranially Iliac muscle Caudally Ileopsoas muscle Iliac bone External iliac vein	Cranially External iliac vein Caudally Public bone (superior branch)	Cranially Ureter Caudally Bladder
Internal iliac nodes	Common iliac bifurcations (about L5-S1 space)	Cranial sections of coccygeal muscle	Bladder Uterus	Cranially Psoas muscle Internal iliac vein Iliac bone Sacroiliac joint Caudally Piriformis m. Internal obturatorius m.	Cranially Sacral wing Caudally Piriform muscle	Mesocolon Uterus Bladder
Obturator nodes	Cranial sections of obturator muscle	Superior margin inferior branch of pubic bone	External iliac vein	Cranially Acetabulum Caudally Internal obturator muscle	Internal obturator muscle	Bladder
Pudendal nodes	Cranial sections of coccygeal muscle	Inferior sections of inferior branch of pubic bone	Cranially Posterior portion of internal obturatorius muscle Acetabulum Caudally Angle between obturator muscle and elevator ani muscle	Cranially Sciatic n. Gluteus m. Caudally internal obturator muscle	Cranially Gluteus muscle Caudally Ischio-rectal fossa fat	Elevator ani mesorectum Elevator ani m.
Deep inguinal nodes	Femoral ring: disappearance of lateral muscles of abdominal wall and artery gets lateral	Ischiatic tuber	Plane on the anterior face of sartorius muscle	Sartorius and ileopsoas mm. Femoral vein Rectum femoris m.	Pectineus m.	Subcutis and pectineus muscle Spermatic cord or round ligament Bladder
Superficial inguinal nodes	Cranial section of sartorius muscle	Section of sartorius and adductor muscles crossing	Subcutis and cutis	Lateral edge of sartorius muscle Subcutis Rectum femoris m. Ileopsoas m.	Femoral vasa Ileopsoas Anterior face of pectineus m. Adductor lungus m. Sartorius m.	Spermatic cord or round ligament Trasversus abd. m. Subcutis Rectus abd. m. Obliquus m. Sovrapubic fat
Presacral nodes	Aortic bifurcation	Coccigeal bone superior edge	Posterior rectum wall	Pyriform muscle	Sacrum	

Abbreviation: CTV = clinical target volume.

means of power injector (model 757 injector SLAS BOLOGNA, Bologna, Italy) at a rate of 3.0 mL/s into an antecubital vein by using an 18-gauge needle was administered.

All patients, by signing an informed consent, accepted that their images could be used for research purposes and the hospital ethics committee permitted this observational study.

In this way, 100 CT scans with 85 enlarged pelvic nodes were selected. Nine slices had more than one enlarged node, eight in the same site (considered as one group), and one had enlarged nodes of two different nodal chains.

Table 1 shows the distribution of CT scans and enlarged nodes recorded according to nodal chains.

At first, CT scans were jointly reviewed by two radiation oncologists (M.P., S.B.) and the two previously mentioned radiologists. Both the most proximal structures to each enlarged node or group of nodes in a clockwise direction (anterior, lateral, posterior, and medial directions) and the number of CT slices where they appeared were recorded (Table 2). Table 2 shows that sometimes the sum of occurrences of recorded structures may be inferior with respect to the number of observed nodes. This occurred because in some cases an anatomic structure appeared as margin of different nodes of the same region and therefore was counted once.

Then, the two radiation oncologists derived guidelines from these observations for nodal CTV drawing. For anterior, lateral, posterior, and medial sides, they chose the most frequent or well-identified structures. In some cases they distinguished cranial and caudal structures if they were different. Furthermore, superior and inferior margins of each nodal chain were determined both on the basis of anatomic origins of the main related arterial vessels and on the basis of their relationship with pelvic structures (8). For example, cranial margins of external and internal iliac nodes are obviously common iliac bifurcations. For superficial inguinal nodes that are not related to vascular structures, the origin of sartorius muscle from anterosuperior iliac spine was established as superior margin and the crossing of the same muscle with adductorius muscle in the upper third of the thigh as inferior margin.

RESULTS

The enlarged nodes or group of nodes were 5 common iliac, 11 external iliac, 5 internal iliac, 6 pudendal, 39 superficial inguinal, 3 presacral, 10 deep inguinal, and 6 obturators.

Table 3 summarizes the observations made for each nodal chain and the number of occurrences of every marginal structures on axial CT slices.

Common iliac nodes had mesocolon and ureter as anterior margin, psoas as lateral and posterior margin, vertebral bone posteriorly, and caval vein medially (Fig. 1).

For enlarged external iliac nodes, subcutaneous fat, small bowel, spermatic cord, and bladder were the most common structures identified anteriorly; iliopsoas muscle and external iliac vein were the more frequent structures at lateral margin; pubic bone caudally and pelvic fat cranially were found as posterior limit; the bladder was the more common medial limit for this nodal chain.

Enlarged internal iliac nodes had bladder as anterior structure; iliac bone with internal obturatorius muscle (m.) and piriformis m. as lateral limit; piriformis m. posteriorly; uterus with bladder and mesorectum as medial structures (Fig. 2).

The margin of pudendal nodes were anteriorly internal obturatorius m. and acetabulum; laterally gluteus m., sciaticus nerve (n.) and internal obturatorius m.; posteriorly, gluteus m. in many cranial slices and caudally ischiorectal fossa fat; and medially, mesorectum in cranial slices and elevator ani in caudal ones (Fig. 3).

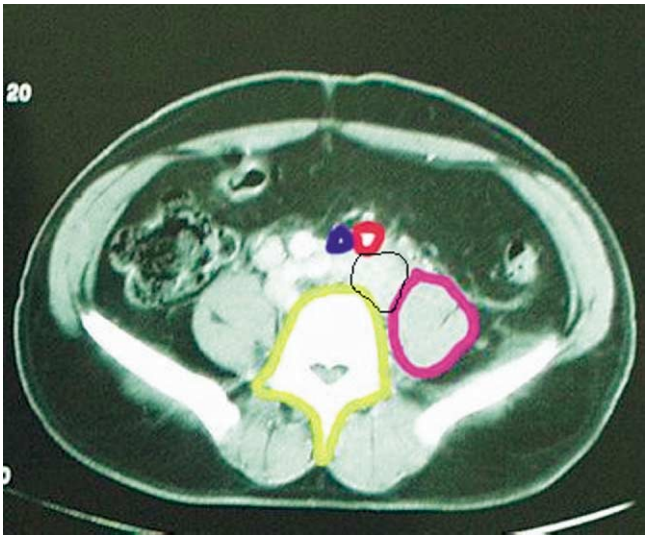

Fig. 1. Common iliac node (black line) in between the psoas muscle (violet), vertebral body (yellow), and common iliac artery (red) just before common iliac bifurcation.

Obturatorii nodes had bladder, uterus, and small bowel anteriorly and medially; obturatorius m. laterally and posteriorly (Fig. 4).

Presacral nodes, lying on anterior sacral face, had posterior rectal wall as anterior limit and piriformis m. as bilateral margins (Fig. 5).

Superficial inguinal nodes had subcutis and sometime cutis as anterior limit, mostly sartorius m. as lateral limit, but some enlarged nodes had sartorius m. (anterior face) and cutis as lateral margin, femoral vessels posteriorly, sper-

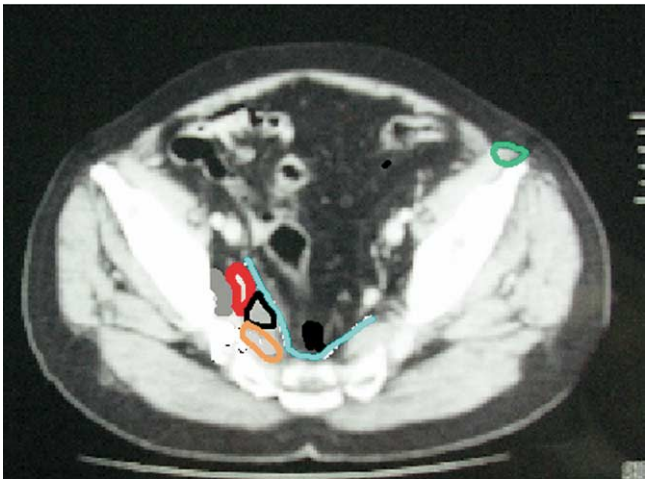

Fig. 2. Internal iliac node (black line) in between the mesocolon (sky blue), piriformis muscle (orange), and iliac vessels (red). Sartorius muscle (green) cranial origin.

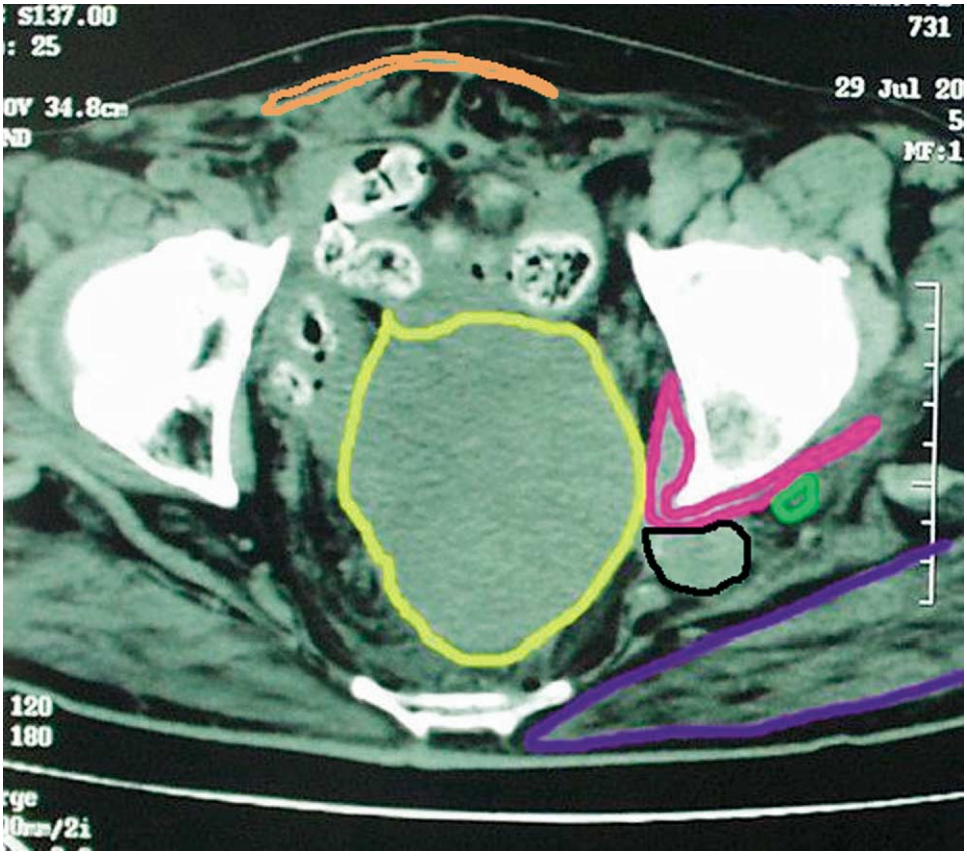

Fig. 3. Pudendal node (black line), obturatorius muscle (purple), sciatic nerve (green), gluteus muscle (violet), and abdominal muscles aponeurosis (orange).

matic cord, or abdominal wall muscles in many cranial slices or subcutis in many caudal ones medially (Fig. 6).

Deep inguinal nodes always appeared medially to femoral vein in a region limited anteriorly by a plane lying on the anterior face of sartorius m., with pectineus m. as posterior and medial margin and spermatic cord and bladder as medial structures (Fig. 7).

On the basis of these data, simple guidelines were derived for node chain CTVs drawing and summarized in Table 3.

DISCUSSION

Both the collection and the review of CT diagnostic exams with enlarged lymph nodes can be very useful in

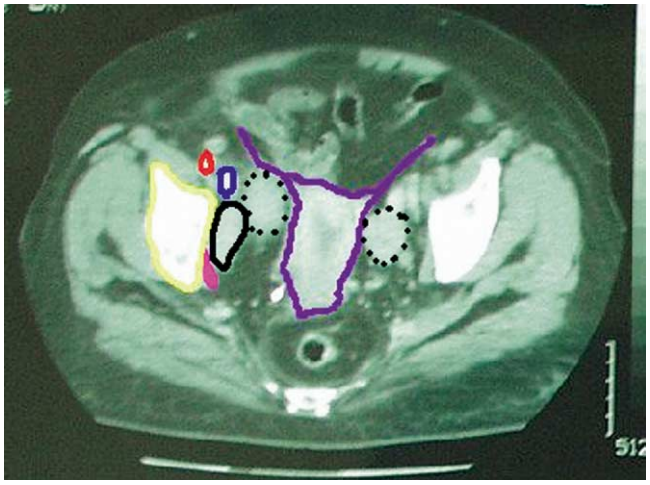

Fig. 4. Obturatorius node (black line), external iliac nodes (dotted black lines), bone (yellow), uterus (violet), obturatorius muscle (purple), iliac vein (blue), and artery (red).

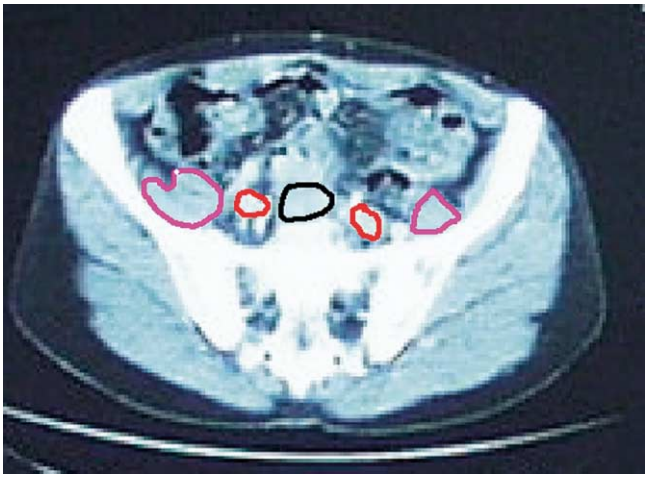

Fig. 5. Presacral nodes (black line), iliac vessels (red), and psoas muscle (purple).

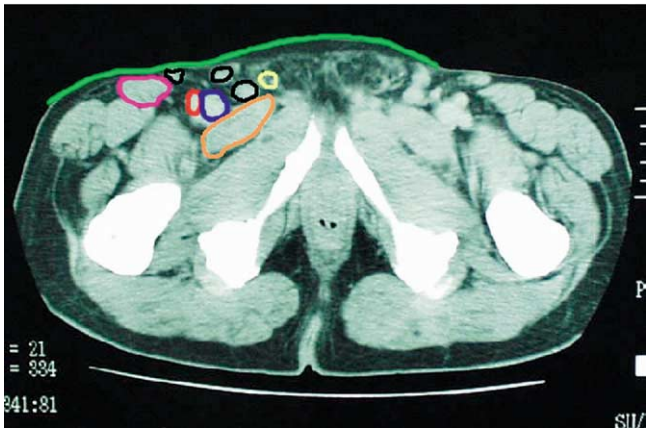

Fig. 6. Superficial inguinal nodes (black lines), inguinal channel (yellow), sartorius muscle (purple), iliac vein (blue) and artery (red), cutis (green), and pectineus muscle (orange).

determining the three-dimensional margins of each pelvic node chain.

Many scientific articles have helped to individualize radiotherapy contouring on CT cross-sections. The efforts to personalize lymph node CTV drawings originated from the surgical measurements of the distance between bilateral external iliac arteries to obtain an accurate wideness of simulation and treatment fields (9). Then, these attempts improved through the definition of the relative position of lymphangiographic images with respect to bony structures by pelvic MRI and lymphangiography (10) and through the classification and topographic description of all body nodes with organ pertinence (11). Finally, radiotherapy succeeded in defining the boundaries of nodal CTV three-dimensionally (5, 6).

Pelvic nodes generally run near the pelvic vessels, which may be easily detected with IVM. The methodology proposed for a correct drawing of nodes in CT pelvis contouring is essentially based on the addition of different margins

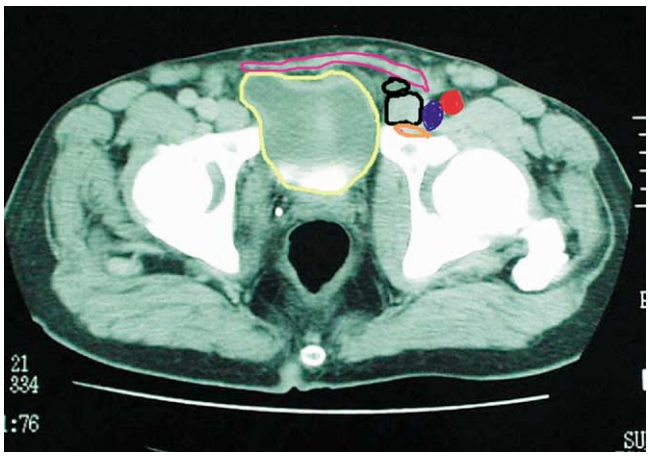

Fig. 7. Deep inguinal nodes (black lines), femoral vein (blue) and artery (red), pectineus muscles (orange), bladder (yellow), and abdominal muscle aponeurosis (orange).

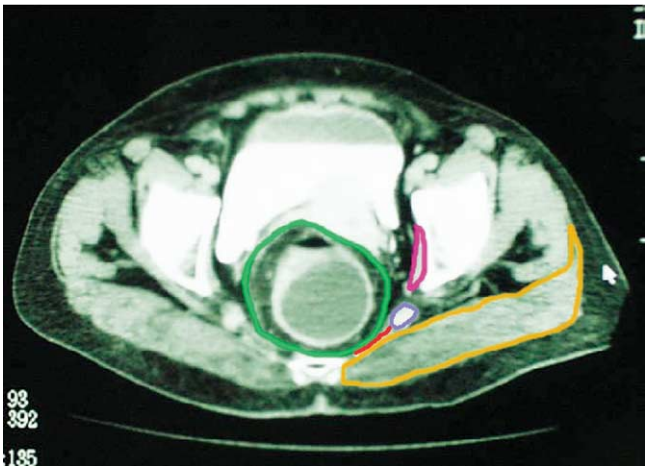

Fig. 8. Coccygeal muscle (red), mesorectum (green), pudendal vessels (violet), obturatorius muscle (fuchsia), and gluteus muscle (orange) at the iliac-pudendal transitional level.

to contrast enhanced vessels: 2 cm (5) or 1 cm, 1.5, and 2 cm according to the artery section with focal expansion (up to >2 cm) and truncation (0.5 cm) (6). These important guidelines associate lymphangiographic with CT images.

But lymphangiography does not always enhance superficial inguinal nodes and obturator nodes. It sometimes enhances internal iliac nodes, but never pudendal nodes.

The method used here has been already adopted in studies for head–and–neck cancer, which recorded sites and rate of nodal recurrences (3). We tried to define the limits of each nodal region in pelvis—independently from risk of recurrence—on cross-sectional CT images.

For a three-dimensional definition of the exact passage from external iliac nodes to inguinal nodes, we attempted to identify constant structures on CT cross-sections. Because of the formation of femoral ring in anterior abdominal wall at the passage of muscle fibers into the aponeurosis of oblique muscle, CT sections, where muscle fibers disappear or where external iliac artery becomes lateral to the vein, were considered as landmarks for the caudal margin of external iliac nodes. Another landmark can be the appearance of the fibers of pectineus muscle (Fig. 7). To determine the passage from internal iliac chains into pudendal chain, the origin of pudendal artery was considered to be just superiorly and laterally to coccygeal muscle (Fig. 8). The cranial section of coccygeal muscles can be therefore considered the lowest margin of internal nodal chains.

The margins definition of superficial inguinal nodes were uncertain for lack of arteries around which the nodes appeared. Enlarged inguinal nodes were detected in cranial sections with respect to femoral ring. Indeed, triangular inguinal space begins soon after sartorius m. starts its trip from anterosuperior iliac spine. The space in question moves with sartorius muscle anteromedially and arrives in the point in which the latter crosses adductor muscles in the thigh (Fig. 2).

Obturatorii nodes follow the posteroanterior course of obturator vessels from internal iliac vessels to obturator

foramina. They occupy cranially a medial position with respect to the internal obturator muscle whereas, caudally they occupy an anterior position.

Some superficial inguinal nodes were found anteriorly to sartorius muscle limited laterally by the angle in between this muscle and cutis (Fig. 6). Medial margins of superficial inguinal nodes are represented by inguinal channel cranially, by the subcutaneous fat of the thigh and by abductor longus muscles caudally.

The objective of this preliminary experience is to introduce a methodology that starts from CT abnormal nodal findings to define the radiologic boundaries of each nodal region.

This study about the relative position of lymph nodes with respect both to soft tissues and bony structures around the vessel pathways may be an invitation toward an exact three-dimensional definition of the margins for pelvic nodal chains.

The guidelines in Table 3 are a monoinstitutional effort to prove the hypothesis to transfer bidimensional information, derived from anatomic and surgical pelvic series, to the three-dimensional "habitat" of CT images for RT planning. They are based on the following assumptions: *(1)* specific radiologic landmarks on CT scans represent the limits of nodal CTV, *(2)* structures frequently detected in proximity to enlarged nodal chain can be chosen for this purpose, and *(3)* enlarged nodes can help identify these landmarks. Certainly, by increasing the number of CT observations, the more accurate will be the choice of the landmarks on the basis of their frequency and visibility. However, there will be individuals for whom guidelines cannot be used on clinical basis. Guidelines contribute to a reduction in the treatment variations from patient to patient. However, they require multi-institutional replication and validation before their general adoption. In conclusion, the preliminary results of this study cannot be generalized, but encourage radiation oncologists to carry out data collection and comparison.

REFERENCES

1. Gregoire V, Coche E, Cosnard G, *et al.* Selection and delineation of lymph node target volumes in head and neck conformal radiotherapy. Proposal of standardizing terminology and procedure based on surgical experience. *Radiother Oncol* 2000;56:135–150.
2. Wijers OB, Levendag PC, Tan T, *et al.* Simplified CT based definition of lymph node levels in the node negative neck. *Radiother Oncol* 1999;52:35–42.
3. Chao KS, Wippold FJ, Ozygit G, *et al.* Determination and delineation of nodal target volumes for head-and neck cancer based on patterns of failure in patients receiving definitive and postoperative IMRT. *Int J Radiat Oncol Biol Phys* 2002;53:1174–1184.
4. Palazzi M, Soatti C, Bianchi E, *et al.* Guidelines for the delineation of nodal regions of the head and neck on axial computed tomography images. *Tumori* 2002;88:355–360.
5. Roeske JC, Luian A, Rotmensh J. Intensity-modulated pelvic radiation therapy in patients with gynecologic malignancies. *Int J Radiat Oncol Biol Phys* 2002;48:1613–1621.
6. Chao KS C, Lin M. Lymphangiogram-assisted lymph node target delineation for patients with gynecologic malignancies. *Int J Radiat Oncol Biol Phys* 2002;54:1147–1152.
7. Landberg T. International Commission on Radiation Units and Measurements. Prescribing, recording and reporting photon beam therapy (Supplement to ICRU 50). ICRU Report 62. Bethesda, MD: ICRU; 1999.
8. Spitzer VM, Whitlock G. Atlas of the viable human male. Sudbury, MA: Jones and Bartlett Publishers; 1996.
9. Greer BE, Koh WJ, Figge DC, *et al.* Gynecologic radiotherapy fields defined by intraoperative measurements. *Gynecol Oncol* 1990;38:421–424.
10. Zunino S, Rosato O, Lucino S, *et al.* Anatomic study of the pelvis in carcinoma of the uterine cervix as related to the box technique. *Int J Radiat Oncol Biol Phys* 1999;44:53–59.
11. Martinez-Monge R, Fernandes PS, Gupta N, *et al.* Cross-sectional nodal atlas: a tool for definition of clinical target volumes in three-dimensional radiation therapy planning. *Radiology* 1999;211:815–828.